



**RLS Calibration Target design to allow onboard combined science between RLS and MicrOmega instruments on the ExoMars rover**

Journal:	<i>Journal of Raman Spectroscopy</i>
Manuscript ID	Draft
Wiley - Manuscript type:	Special Issue - Research Article
Date Submitted by the Author:	n/a
Complete List of Authors:	<p>Lopez-Reyes, Guillermo; Centro de Astrobiología, Unidad Asociada UVA-CSIC          Pilorget, Cedric; Universite Paris-Sud, Institut d'Astrophysique Spatiale Moral, Andoni; INTA (Instituto Nacional de Técnica Aeroespacial), Programas Espaciales          Manrique, Jose ; Universidad de Valladolid, Condensed Matter Physics, Crystallography and Mineralogy          Sanz, Aurelio; University of Valladolid, Unidad Asociada UVA-CSIC al Centro de Astrobiología          Berrocal, Alicia; Isdefe, INTA          Veneranda, Marco; University of Valladolid, Condensed Matter Physics, Crystallography and Mineralogy          Rull, Fernando; University, Física Materia Condensada          Medina-García, Jesus; Centro de Astrobiología, Unidad Asociada UVA-CSIC          Hamm, Vincent; Universite Paris-Sud, Institut d'Astrophysique Spatiale          Bibring, Jean-Pierre; Universite Paris-Sud, Institut d'Astrophysique Spatiale          Rodriguez, José A.; ISDEFE (Ingeniería de Sistemas para la Defensa de España, S.A, ISDEFE, C. Beatriz de Bobadilla, 3, 28040 Madrid, Spain) as external contractor for INTA, ISDEFE          Perez, Carlos; INTA (Instituto Nacional de Técnica Aeroespacial), Programas Espaciales          Mateo-Marti, Eva; Centro de Astrobiología, Planetología y habitabilidad          Prieto-Ballesteros, Olga; Centro de Astrobiología, Planetología y Habitabilidad          Lalla, Emmanuel; York University, Centre for Research in Earth and Space Science          Vago, Jorge; ESA, ExoMars Programme Scientist Science and Robotic Exploration Directorate</p>
Keywords:	Combined science, Calibration Target, Raman spectroscopy, Infrared spectroscopy, ExoMars

SCHOLARONE™  
Manuscripts

1  
2  
3  
4  
5  
6  
7  
8  
9  
10  
11  
12  
13  
14  
15  
16  
17  
18  
19  
20  
21  
22  
23  
24  
25  
26  
27  
28  
29  
30  
31  
32  
33  
34  
35  
36  
37  
38  
39  
40  
41  
42  
43  
44  
45  
46  
47  
48  
49  
50  
51  
52  
53  
54  
55  
56  
57  
58  
59  
60

# 1 RLS Calibration Target design to allow onboard combined science 2 between RLS and MicrOmega instruments on the ExoMars rover

3 Guillermo Lopez-Reyes<sup>1</sup>, Cedric Pilorget<sup>2</sup>, Andoni G. Moral<sup>3</sup>, Jose Antonio  
4 Manrique<sup>1</sup>, Aurelio Sanz<sup>1</sup>, Alicia Berrocal<sup>4</sup>, Marco Veneranda<sup>1</sup>, Fernando Rull<sup>1</sup>,  
5 Jesús Medina<sup>1</sup>, Vincent Hamm<sup>2</sup>, Jean-Pierre Bibring<sup>2</sup>, Jose Antonio Rodriguez<sup>4</sup>,  
6 Carlos Perez Canora<sup>3</sup>, Eva Mateo-Marti<sup>5</sup>, Olga Prieto-Ballesteros<sup>5</sup>, Emmanuel Lalla<sup>6</sup>  
7 and Jorge L. Vago<sup>7</sup>

8 <sup>1</sup>Unidad Asociada UVa-CSIC-CAB, C/ Francisco Valles 8, 47151, Valladolid (Spain), <sup>2</sup>IAS, Univ. Paris-  
9 Sud, 91405 ORSAY CEDEX (France), <sup>3</sup>Instituto Nacional de Técnica Aeroespacial (INTA), Crtra. Ajalvir  
10 Km.4, 28850, Torrejón de Ardoz (Spain), <sup>4</sup>ISDEFE, Crtra. Ajalvir Km.4, 28850, Torrejón de Ardoz  
11 (Spain), <sup>5</sup>Centro de Astrobiología (CAB), Crtra. Ajalvir Km.4, 28850, Torrejón de Ardoz (Spain), <sup>6</sup>Centre  
12 for Research in Earth and Space Science, York University, Toronto (Canada), <sup>7</sup>ESA-ESTEC, Noordwijk  
13 (the Netherlands).

14 E-mail: [guillermo.lopez@cab.inta-csic.es](mailto:guillermo.lopez@cab.inta-csic.es)

## 15 Abstract

16 The ExoMars rover will be launched in 2020 with several instruments that will be able to  
17 perform combined science between instruments, for the first time allowing the instruments  
18 to analyze the same spots of the same samples. The Raman Laser Spectrometer (RLS)  
19 instrument Calibration Target (CT) includes a polyethylene terephthalate (PET) calibrant  
20 that has been subject to a series of tests to qualify it for space and to properly characterize  
21 its behavior during mission, in order to be used by RLS for the verification of the instrument  
22 calibration and health status. In addition, the RLS CT includes some patterns that the  
23 instruments will detect and that will be used to establish their relative positions, thus  
24 becoming a key element in order to facilitate the spatial correlation of the instruments, and  
25 thus the combined science. The results from the joint tests performed by the RLS and  
26 MicrOmega instruments support the operational approach designed for the ExoMars rover,  
27 which allows complementing the necessary collaborative science onboard ExoMars with  
28 the autonomous RLS operation.

29 **Keywords:** Combined science, Calibration Target, Raman spectroscopy, Infrared  
30 spectroscopy, Exomars

## 31 Introduction

32 The ExoMars mission of the European Space Agency (ESA) will send a rover to Mars in 2020  
33 with the main objective of providing insight to the present or past existence of life in the red  
34 planet <sup>[1]</sup>. Compared to other Mars missions such as the Mars Exploration Rovers Spirit and  
35 Opportunity, the NASA Mars Science Laboratory (MSL) rover Curiosity, or even the Mars  
36 2020 rover mission to be sent to Mars by NASA at the same time as ExoMars, the European  
37 rover will feature two unique capabilities unprecedented on the exploration of Mars. On one  
38 side, the capability of analyzing samples from the subsurface down to depths of two meters,  
39 where the potential organic material is not affected by the ionizing radiation received at the  
40 surface. On the other hand, the ExoMars rover includes a laboratory with a sample carousel  
41 that will allow the analysis of the same sample, in the same spots, by different instruments.  
42 These two features constitute an important step forward for in situ analyses on Mars, as  
43 they provide the real possibility of analyzing potential organic material present on the

1  
2  
3 44 planet's surface, while allowing the instruments to verify and complement each other  
4 45 results by analyzing the exact same areas of the sample, at micrometric scale.

6 46 These features are possible in the ExoMars rover<sup>[1]</sup> thanks to the nested-investigations  
7 47 concept design, which allows it to analyze from panoramic to molecular scale with its  
8 48 Pasteur Payload, as it incorporates instruments and systems capable of performing nested  
9 49 experiments, from the panoramic cameras to spectroscopic and molecular analysis,  
10 50 including also the necessary sample extraction and preparation. Concretely, the rover  
11 51 includes a subsurface drill capable of extracting samples from the shallow subsurface of  
12 52 Mars, down to a depth of two meters. The collected materials are then crushed and served  
13 53 to the instruments of the Analytical Laboratory Drawer (ALD) in a carrousel with the  
14 54 Sample Preparation and Distribution System (SPDS). This system includes a Refillable  
15 55 Container (RC) in which the crushed sample will be placed and flattened. The instruments  
16 56 in the ALD will then be able to analyze a flat surface of the powdered sample when the RC  
17 57 is placed by the carrousel below them. This allows analyzing the same sample surface with  
18 58 several complementary techniques, such as Raman spectroscopy (RLS)<sup>[2]</sup>, visual plus  
19 59 infrared spectroscopy (MicrOmega-MICR)<sup>[3-5]</sup> and laser desorption mass spectrometry  
20 60 LDMS (MOMA)<sup>[6]</sup>, instruments forming part of the ALD.

24 61 The capability of the ExoMars rover to analyze the same sample with the different  
25 62 instruments of the ALD provides the possibility of performing combined or cooperative  
26 63 science between the analytical systems. The sample characterization will be performed  
27 64 sequentially by the three instruments of the ALD, starting with MicrOmega, followed by RLS,  
28 65 and then MOMA LDMS. This means that it is possible to take the previous instrument  
29 66 analytical results in consideration to improve the analysis of the next, to do some kind of  
30 67 "directed" sample characterization (e.g. analyzing a spot that is considered interesting by a  
31 68 previous instrument) in addition to the automated analysis performed by each instrument.  
32 69 Concretely, this analytical concept has been implemented onboard the rover software, to  
33 70 allow the automated cooperative science between RLS and MicrOmega, even without the  
34 71 intervention of operators, while also respecting the automated operation of each  
35 72 instrument. The cooperative analysis with MOMA LDMS will require a previous study by the  
36 73 scientists on ground.

39 74 MicrOmega provides a measurement field of view (FoV) of  $\sim 5 \times 5 \text{ mm}^2$  <sup>[3]</sup>. RLS performs  
40 75 micro Raman studies along a line traced by the carrousel with a 50 microns spot<sup>[2]</sup> and  
41 76 MOMA LDMS presents a spot size of  $\sim 400$  microns<sup>[6]</sup>, with a central effective size of around  
42 77 150 microns. Given the differences among the instruments FoVs, it is of paramount  
43 78 importance to ensure the mechanical alignment between the different instruments,  
44 79 especially between RLS and MicrOmega, given the possibility of performing automated  
45 80 combined science. In this sense, the RLS instrument features a Calibration Target (CT) that  
46 81 has been implemented with features that are detectable both by the RLS and MicrOmega  
47 82 instruments to both facilitate the calibration verification of the RLS instrument, as well as  
48 83 the spatial cross-registration between both instruments.

52 84 The Raman Laser Spectrometer (RLS) <sup>[2]</sup> is a Raman spectrometer with a continuous wave  
53 85 excitation laser with a wavelength of 532 nm and a power between 10 and 20 mW, with a  
54 86 spot size on the sample of 50 microns. The spectrometer has a spectral range between 533  
55 87 and 676 nm, with a spectral resolution between 6 and 8  $\text{cm}^{-1}$ . The optical head of the  
56 88 instrument provides autofocus capabilities, establishing the focus position based on the  
57 89 intensity of the signal reflected on the sample. To do so, the laser includes a photodiode  
58 90 which measures the reflected light on the sample, providing higher intensity when the  
59 91 sample is better focused. Based on this intensity, the autofocus algorithm implemented will

92 move the optical head lens to modify the focus position, searching for the maximum  
93 intensity.

94 The RLS instrument includes two Calibration Targets in the ultra-clean zone (UCZ) of the  
95 rover, these being placed on the carousel that positions the Martian samples. These CTs  
96 have a double function: 1- to ensure and verify the calibration status of the instrument and  
97 2- to ensure the spatial cross-registration of the MicrOmega and RLS instruments inside the  
98 ALD. The reason behind the presence of two CTs for RLS is an operational constraint, which  
99 makes it impossible to have a CT under the RLS instrument during cruise without affecting  
100 the sample surface during operation on Mars after the analysis with MicrOmega. By using 2  
101 CTs it is possible to guarantee the presence of a CT under RLS during cruise, while allowing  
102 the RLS calibration to happen before the Raman acquisition of the Martian sample already  
103 analyzed by MicrOmega.

104 The two RLS CTs are not identical. Even if their base material and design is the same, one of  
105 them is equipped with some laser and mechanically-performed patterns that are visible  
106 both by MicrOmega and RLS, allowing the cross-registration of the sample area that RLS will  
107 analyze with respect to the MicrOmega FoV.

108 In this paper, the objective is double. On one hand, the RLS CT design is described to show  
109 how it fulfills both the requirements of allowing a proper verification of the RLS calibration  
110 while surviving the harsh conditions of space and space qualification and its expected  
111 performance, as well as providing a means for the spatial cross-registration of RLS and  
112 MicrOmega FoVs. On the other hand, the paper addresses how the combined science  
113 improves the scientific return of the mission by describing some joint tests and experiments  
114 already performed in the framework of the ExoMars mission with other instruments of the  
115 ALD, specifically, between RLS and MicrOmega.

## 116 **The Calibration Targets of the RLS instrument**

### 117 *RLS CT design for the verification of the RLS health status*

118 The two RLS CTs included in the ExoMars rover (Figure 1b) are placed on the same  
119 carousel that will host Martian sub-surface samples, allowing the calibration of the  
120 instruments by turning the carousel and placing the corresponding CT under the  
121 instrument probe. Given that the CTs are placed in the UCZ of the rover, and the proximity  
122 to very low-threshold detection instruments such as MOMA GCMS, the cleanliness and  
123 contamination requirements are extremely tight, and unprecedented in any other previous  
124 mission to another planetary body. This limits the quantity of organic materials to be used  
125 for the CT, but also implies very hard cleaning and sterilization methods, including bakeouts  
126 at very high temperatures (>110°C). The requirements imposed to the RLS CTs included, in  
127 addition, a very low outgassing rate, to have multiple peaks evenly distributed along the  
128 spectral range of the instrument, small mass (less than 20 mg), compatibility with  
129 sterilization temperatures (>110°C) and organic solvents, stable behavior in large  
130 temperature ranges (-50°C to 40°C), resilience to ultra-violet radiation, etc.

131 The main requirement for the selection of the material was to survive a wide range of  
132 temperatures while providing multiple peaks evenly distributed along the spectral range,  
133 as shown in Figure 1a. Many mineral and organic materials were tested and, according to  
134 the obtained results, Polyethylene Terephthalate (PET)<sup>[7]</sup> was chosen as optimal candidate.  
135 This same material has also been selected as part of the payload on the NASA Mars 2020  
136 SuperCam Calibration Target.

1  
2  
3 137 As previously stated, the requirements for organic material inside the UCZ of the rover were  
4 138 extremely tight, with both CTs using a total mass of PET <20 mg. In order to fix this small  
5 139 quantity of calibration material to the rover carousel, a configuration as shown in Figure  
6 140 1c is used. The calibrating material consists of a PET hat-like disk with a visible surface of  
7 141 2.4 mm diameter. The main body of the mechanical assembly is aluminum coated with  
8 142 Iridite 14-2, a chromate conversion coating to guarantee a good behavior against corrosion.  
9 143 The PET is then mechanically fixed to the main body by means of a stainless-steel cap which  
10 144 is screwed on top of the main body.

11  
12  
13 145 In order to verify the compliance with the requirements imposed to the CT, as well as to  
14 146 have a proper characterization of the calibration material together with some insight on the  
15 147 potential evolution of the CT spectral response in the expected environment on Mars,  
16 148 several tests were performed.

17  
18 149 PET was tested at different temperatures in the operational range of the mission, to verify  
19 150 the spectral response of the polymer in the actual operation conditions. This analysis was  
20 151 performed by acquiring spectra of the PET inside a small thermal chamber at ambient, 0°C  
21 152 and -20°C temperatures, in a 40 mbar vacuum environment. The results showed that, in  
22 153 terms of peak positions, the potential variations of the spectrum at different temperatures  
23 154 are negligible when analyzed with the RLS instrument, while there is a trend of signal-to-  
24 155 noise ratio (SNR) decrease (between 15% and 35% depending on the analyzed spot) when  
25 156 temperature falls from 293 to 253°K.

26  
27  
28 157 Outgassing tests (both static and dynamic) provided values in line with the mission  
29 158 requirements. In addition, a very long (150h) bakeout at 125°C in vacuum was performed  
30 159 on the PET to ensure a proper degasification of the material included in the UCZ, as well as  
31 160 a final sterilization process of the complete assembly of 120h at 115°C. The preliminary  
32 161 tests performed on the selected PET at those temperatures showed no modifications in the  
33 162 spectral profile before and after, except for a slight increase on the background signal.  
34 163 Considering that the baking temperature is higher than the glass transition temperature of  
35 164 the selected PET, the background increase can probably be related to a slightly worse  
36 165 ordered recrystallization of the polymer. High cooling temperature slopes, however,  
37 166 showed to result in higher disordered structures than slow cooling, so, by controlling the  
38 167 cooling slope, the resulting PET was little affected by the very high temperatures. Taking all  
39 168 this into consideration, the procedures for the qualification were properly adjusted. During  
40 169 the qualification campaign, two different ovens were used for three test units. Two were  
41 170 baked in the same oven as the delivered units (CT3 and CT4), and one in the second oven  
42 171 (CT5) due to a lack of space. Then, the PET of the three units were analyzed with Raman  
43 172 before and after the qualification campaign, obtaining the results depicted in Table 1. This  
44 173 characterization was done with constant acquisition parameters, concluding that there was  
45 174 no SNR loss after the baking, and that even for CT3 and CT4 the SNR was even better  
46 175 (explained by a slightly better crystallization due to the difference in the cooling curve of  
47 176 the two ovens).

48  
49  
50  
51  
52 177 The ultra-violet (UV) radiation on Mars has been thoroughly studied and investigated in-  
53 178 situ<sup>[8]</sup> and is dependent on many factors such as latitude, season<sup>[9]</sup>, suspended powder in  
54 179 the atmosphere<sup>[10]</sup>, etc. In any case, it is higher than on Earth, thus potentially highly  
55 180 affecting the organic materials present on the Martian surface. The RLS CT will be enclosed  
56 181 behind several metallic layers in a very dark environment that will protect the internal parts  
57 182 from the ionizing radiation. Nevertheless, a test was performed by means of the PASC  
58 183 chamber<sup>[11,12]</sup> which simulates the environmental conditions of Mars, including UV  
59 184 radiation. A 1cm diameter, 5mm thick PET sample extracted from the RLS CT PET batch was



1  
2  
3 185 subjected to a continuous source of UV illumination for 130h with an irradiance on the  
4 186 sample of 30 W/cm<sup>2</sup>. The total dose applied to the samples was the same as the expected  
5 187 equivalent dose received by the ExoMars rover during its nominal mission (140 sols),  
6 188 considering the calculated UV flux at the Martian equator<sup>[13]</sup>, and approximating the values  
7 189 with the latitude of Oxia Planum, landing site of ExoMars. The results of the experiment  
8 190 showed a slight modification in the coloration (yellowish tone) of the PET (which is white)  
9 191 in the exposed areas. However, the spectral signature of the PET seemed quite unaffected  
10 192 in terms of peak positions and intensities. The SNR, however, was negatively affected by the  
11 193 radiation effects, as shown in Table 2. All peaks were nevertheless detectable. Considering  
12 194 the results of the test, the UV incidence on the CT was considered of minor importance, given  
13 195 that all the relevant spectral features are detectable and especially considering that the PET  
14 196 part will be safe from the UV radiation in the interior of the rover ALD. However, these  
15 197 results have also been useful for the selection of PET as part of the SuperCam Calibration  
16 198 Target onboard the Mars 2020 mission, which is external and thus exposed to the Martian  
17 199 environment. This sample on the SCCT is also aimed at the study of the evolution of organics  
18 200 in the Martian environment.

19 201 The set of tests performed as part of the RLS CT development and qualification campaign  
20 202 are aimed at characterizing the calibrant (PET) spectral response for the proper  
21 203 characterization of the instrument by comparing both the background intensity and peak  
22 204 spectral response on ground, vs. along the mission span. These tests offered a thorough  
23 205 understanding of the expected behavior of the calibration target PET once on the surface of  
24 206 Mars, providing the means to help understand the RLS instrument end to end performance  
25 207 during operation.

#### 26 208 *RLS CT design for spatial cross-registration with MicrOmega*

27 209 Given the different scales of FoV between the different instruments (the MicrOmega FoV of  
28 210 ~5x5 mm<sup>2</sup> while the RLS instrument can access a 50 microns thick line), it is actually  
29 211 impossible to know precisely the relative positions of the corresponding FoVs based only  
30 212 on the mechanical alignment of the rover parts, as the mechanical uncertainty due to the  
31 213 manufacturing tolerances and thermal effects is in the order of magnitude of the RLS FoV.  
32 214 Thus, it is not possible to exactly establish the relative positions of the instruments  
33 215 beforehand. It is also not possible to measure it afterwards given that, once the UCZ is closed  
34 216 mounted, it is no longer possible to access the internal part of the UCZ to measure the  
35 217 relative positions of the instruments.

36 218 Thus, the only alternative is to use the instruments themselves to calculate their relative  
37 219 position, which can be done by analyzing the same known sample. In this case, it was  
38 220 decided that the RLS CT would be said known sample. For the RLS CT to be visible by  
39 221 MicrOmega, several characteristic features were introduced in one of the RLS CTs, so these  
40 222 features could be used by MicrOmega to univocally identify the RLS path (of course, the RLS  
41 223 instrument will need to analyze these features as well) on the MICR FoV, and thus their  
42 224 relative positions. This will then allow the combined science between the instruments,  
43 225 providing the possibility of precisely moving the rover carousel so the RLS instrument is  
44 226 able to analyze a spot previously analyzed by MicrOmega.

45 227 The RLS CT design includes two different types of marks –mechanical and laser-induced,  
46 228 see Figure 2a and b– in order to benefit from the different inputs obtained by the RLS  
47 229 instrument: concretely, the RLS instrument can analyze the molecular composition of a  
48 230 sample in base of its Raman spectrum, but also can use the autofocus photodiode to identify  
49 231 the focus position, based on the intensity received from the reflected light. The laser-

232 induced marks inflict a modification of the molecular structure of the PET that is detected  
233 with Raman spectroscopy, while the CT surface is mechanically milled in two different  
234 planes, with a mechanical step of 70 microns.

235 The laser marking consists of a pattern of three unparallel lines (they are rotated -15 and  
236 +20° each with respect to the central line) crossing the PET disk transversally to the  
237 carousel moving direction, so the instrument will cross over the lines. The laser marks are  
238 induced using a Datalogic Ulyxe laser marking system. The molecular structural  
239 modification caused by the laser on the lines is easily detected by Raman spectroscopy.

240 The mechanical milling of the PET was performed by a numerical milling machine with a 30  
241 microns diameter mill, creating a pattern on the surface of the PET as shown in (Figure 2a  
242 and b), with a depth of 100 microns. As a result, two sample planes at different heights with  
243 slightly different surface rugosities are observed. This is convenient as the RLS will be able  
244 to detect the height differences between one plane and the other, and MicrOmega will be  
245 able to identify the different rugosity of both surfaces.

246 These characteristics make that both the RLS and MicrOmega instruments can analyze the  
247 characteristic features of the RLS CT, in order to univocally know the relative positions of  
248 the instruments, favoring the combined science on the ExoMars mission.

### 249 **Combined science between MicrOmega and RLS**

250 The ExoMars rover presents, for the first time in the robotic exploration of Mars, a suite of  
251 instruments capable of analyzing the same samples, in the very same spots at a micrometric  
252 scale. This is achieved thanks to the carousel concept implemented on the rover, which will  
253 sequentially place the Martian powdered-sample below the MicrOmega, RLS and MOMA  
254 LDMS instruments. This will provide a unique opportunity to perform combined science  
255 among the different instruments of the rover.

256 Given the intrinsic differences on the FoVs of the instruments, MicrOmega (FoV ~5x5 mm<sup>2</sup>)  
257 will be able to analyze both the RLS (50 microns spot) and MOMA LDMS (~150 microns  
258 effective spot) sample paths, being the spatial cross-registration of the relative positions  
259 necessary for MOMA-MicrOmega, and RLS-MicrOmega. However, given the micrometric  
260 scale of their FoVs, there is a high chance that the RLS and MOMA LDMS paths do not overlap  
261 on the same sample spot.

262 The rover software operation concept foresees the possibility of performing an autonomous  
263 combined science between MicrOmega and RLS, with the RLS analyzing interesting spots  
264 detected by MicrOmega (the interest of these regions being automatically estimated  
265 onboard following the guidelines of the ExoMars scientific team). This implementation is  
266 based on the fact that the RLS and MicrOmega instruments might operate during the same  
267 sol, without any possibility of ground intervention. The MOMA LDMS analysis, on the other  
268 hand, will happen in a different sol than RLS and MicrOmega. Thus, the MOMA team will be  
269 able to use both MicrOmega and RLS inputs to define their operation strategy. For these  
270 reasons, on this paper, the focus is placed on the MicrOmega-RLS combined science.

### 271 *Spatial cross-registration of MicrOmega and RLS*

272 The characteristic features implemented in the RLS CT will be analyzed and detected during  
273 the initial phases of Mars operation by MicrOmega and RLS in order to establish the relative  
274 positions between the MicrOmega and RLS instrument, facilitating the detailed  
275 characterization of the spatial correlation necessary for the combined science.



1  
2  
3 276 The RLS instrument detects the CT features in two different ways. 1- The laser marks are  
4 277 detected based on their Raman signature, given that the matrix material (PET) molecular  
5 278 structure is modified by the laser and thus is detectable with the spectrometer. The spectral  
6 279 effect is given by a high increment on the background signal of the spectrum, as shown in  
7 280 Figure 3a. Even if the transition between the PET and the laser mark is not totally abrupt,  
8 281 by analyzing the acquired spectra it is possible to decide if the acquired spectrum  
9 282 corresponds to a marked or unmarked part of the CT. Figure 3b shows how the  
10 283 approximated width at half maximum of the curve obtained by integrating the spectra areas  
11 284 is representative of the thickness of the line (between 80 and 100 microns). 2- The  
12 285 mechanical marks, which provide two different planes on the CT surface, can be identified  
13 286 as well based on the spectral features, but also by means of the RLS autofocus photodiode,  
14 287 which measures a higher intensity of the reflected light when in focus (see Figure 3c).

15  
16  
17 288 Then, by measuring the distance between laser and mechanical marks, it will be possible to  
18 289 know the position of the path of analysis on the rover carrousel.

19  
20  
21 290 In order to test the RLS capabilities to detect the CT features, as well as to properly  
22 291 characterize the flight CT, a complete Raman mapping of the CT was performed with the  
23 292 RLS ExoMars Simulator<sup>[14-16]</sup>, covering the complete CT surface in steps of 20 microns,  
24 293 acquiring a spectrum at each spot with a fixed integration time, adding a total of more than  
25 294 12 thousand spectra. The representation in Figure 4 shows, at each pixel, the spectrum  
26 295 integrated area in the corresponding position of the CT surface. It is easily observed how  
27 296 the laser marks are very clearly detected, as are the borders between the upper and lower  
28 297 planes of the CT.

29  
30  
31 298 To test the autofocus photodiode capability of detection of the mechanical marks, the RLS  
32 299 FM was used and several lines were swept on the CT, acquiring three housekeeping values  
33 300 from the autofocus photodiode at each point. The result showed (see Figure 5) that the  
34 301 housekeeping data from this photodiode will complement the Raman analysis for the  
35 302 characterization of the path followed by the instrument.

36  
37 303 The RLS CT has also been analyzed with the MicrOmega EQM, which provides a 5x5 mm<sup>2</sup>  
38 304 FoV with a spatial sampling of 40 microns. The flight version that will operate on Mars has  
39 305 also a 5x5 mm<sup>2</sup> FoV, but with a spatial sampling of 20 microns.

40  
41 306 The analysis with MicrOmega shows that both the milled part of the CT and the laser marks  
42 307 can be properly identified. In particular, the analysis of the monochromatic images shows a  
43 308 reflectance contrast at the edges of the milled parts (Figure 6a and b). The roughness  
44 309 differences between both planes, and in particular the marks made by the milling, can be  
45 310 observed and used to retrieve the pattern drawn on the CT. The laser marks can also be  
46 311 distinctively seen on the monochromatic images (Figure 6a and c). In addition to the  
47 312 reflectance contrast, that by itself enables to identify both the edges of the milled parts and  
48 313 the laser marks, it can be observed that the reflectance spectra exhibit different features  
49 314 over the areas that were shot by the laser, highlighting a modification of the surface  
50 315 composition of the PET material (Figure 6d and e). The laser marks can thus also be detected  
51 316 by MICR using the spectral dimension of the dataset, which provides an additional and  
52 317 potentially more robust identification means than simple albedo difference. Using the latter  
53 318 technique, laser marks, as seen by the MicrOmega unit, are typically 2-4 pixels large,  
54 319 corresponding to 50-100 microns, in agreement with the laser marks thickness.

55  
56  
57  
58 320 Based on the detection of the patterns by MicrOmega and RLS, it will be possible to assess  
59 321 where on the MicrOmega FoV will the path of analysis of RLS be. This exercise will be done  
60

3 322 during the calibration phase on Mars, getting their spatial cross-registration to ensure  
4 323 successful combined science experiments on the ExoMars rover on Mars.

6 324

8 325 *Combined operation RLS-MicrOmega*

9 326 Joint test with MicrOmega EQM

11 327 MicrOmega and RLS will provide complementary mineralogical information about the  
12 328 sample composition as well as first order characterization of organics if present. MOMA  
13 329 targets more specifically volatiles, in particular organics, with a very high sensitivity, and is  
14 330 able to give quantitative information about their chemical composition. Compounds of  
15 331 major interest (e.g. organics, phyllosilicates, carbonates) are expected to be minor within  
16 332 the samples and localized in specific spots. Sequential analysis of these specific locations by  
17 333 all three techniques will be required in order to achieve an in-depth characterization, in  
18 334 particular investigate the potential organic content associated to some specific mineral  
19 335 phases. It thus constitutes a key aspect to reach the scientific objectives of the mission.

22 336 These combined analyses can be performed by using MicrOmega capability to first  
23 337 characterize the sample composition over a large area, and then provide the location of  
24 338 targets of interest to RLS and MOMA through the use of automated algorithms<sup>[17]</sup> onboard  
25 339 the rover.

27 340 In this section we describe a test that simulates this protocol, in a joint test with the  
28 341 MicrOmega<sup>[3]</sup> EQM and the RLS ExoMars Simulator<sup>[14]</sup>, which can simulate the carousel  
29 342 motion with its two-axis positioning stage.

31 343 Two samples were selected for the combined science test. Sample 1 is a mixture of different  
32 344 salts (carbonates and sulfates) and phyllosilicates, with a grain size distribution ranging  
33 345 from a few microns to ~315 microns. Sample 2 corresponds to a mixture of olivine  
34 346 (forsterite and fayalite) with carbonates, with a grain size distribution ranging from a few  
35 347 microns to ~315 microns. In particular, a few grains of dolomite were added atop the  
36 348 sample once put in the sample container. The samples mass compositions are detailed in  
37 349 Figure 7.

40 350 The test sequence consisted on placing the sample under the MicrOmega FoV, and then  
41 351 running a typical science sequence (320 science channels covering the 0.99-3.6  $\mu\text{m}$  range).  
42 352 Then the algorithms for detection of interesting spectral features were run. During this test,  
43 353 carbonates were specifically targeted within the samples. These compounds are linked to  
44 354 the evolution of the Martian atmosphere and climate and are thus key targets to understand  
45 355 the processes related to liquid water, being good candidates for the combined science test.  
46 356 After detection of the interesting spots, these spots are placed under the RLS instrument for  
47 357 analysis. Finally, and for comparison, a blind test is performed by the RLS instrument on the  
48 358 powdered sample (fully automated analysis without taking into consideration the  
49 359 MicrOmega results)

52 360 The combined science analysis on sample 1 showed that MicrOmega detected a few spots  
53 361 rich in carbonates, their corresponding coordinates being extracted from the MicrOmega  
54 362 data (Figure 8 and Table 3). Then, the targets were positioned for RLS on the calculated  
55 363 spots, obtaining the results on the corresponding center positions of the detected clusters  
56 364 shown in Figure 8b. In this case, MicrOmega detected the presence of carbonate signatures  
57 365 while RLS detailed the corresponding mineral phase (Figure 8d), highlighting the  
58 366 complementarity between these two spectroscopic techniques. Table 3 summarizes all the

1  
2  
3 367 results. The automated (blind) analysis performed by the RLS instrument provided the  
4 368 results shown in Figure 8e. In this analysis, the RLS instrument was capable of detecting all  
5 369 the mineral phases found in combined mode, in several cases with better spectral quality.  
6 370 In addition, RLS found traces of anhydrite, supposedly not present on the sample, but  
7 371 probably transitioned from gypsum after some process of dehydration.

8  
9 372 The analysis of sample 2 by MicrOmega detected some spots rich in carbonates (anhydrous  
10 373 and OH/H<sub>2</sub>O rich carbonates), and the corresponding coordinates of a few targets were  
11 374 extracted from the MicrOmega data (Figure 9a, b and c). As the criterion for carbonate  
12 375 detection also works for organics, the small (1-2 pixels) and widespread spots identified by  
13 376 the algorithms and associated to olivine, are interpreted to be organics that were in the  
14 377 olivine samples.

15  
16  
17 378 After the MicrOmega test, the selected sample spots were placed under the RLS instrument.  
18 379 Differently from sample 1, in this case, instead of performing a unique spectrum on the exact  
19 380 spot, a 9-point analysis was performed with the RLS instrument. The calculated spot placed  
20 381 in the center of a 3-by-3 grid for target A, with 100-micron steps. For Targets B to D, the  
21 382 calculated spot was placed in the center of a 9-point line with 50-micron steps. Figure 9d  
22 383 shows a summary of the detected mineral phases by RLS on the spots indicated by  
23 384 MicrOmega. In addition, an 8-point automated (blind) analysis was performed by RLS (note  
24 385 that the standard automated test for RLS acquires at least 20 points). The results of this  
25 386 analysis are shown in Figure 9e. The automated analysis of RLS on this type of sample, with  
26 387 only 8 points, was able to detect the three mineral phases present in the mixture (two types  
27 388 of olivine and dolomite). The summary of results is covered in Table 4.

28  
29  
30 389 The results of the analysis of sample 1 highlight the importance of the collaborative science  
31 390 between the different instruments: placing the RLS instrument directly on an interesting  
32 391 grain in a matrix of other materials has allowed detecting that material very easy and  
33 392 accurately. Furthermore, due to the inherent characteristics of infrared vs Raman  
34 393 spectroscopy, the analysis with RLS provides a more accurate identification of the mineral  
35 394 phases present in the sample, in comparison with MicrOmega. The analysis of sample 2  
36 395 again highlights the necessary improvement in terms of science return of the combined  
37 396 science between the different instruments of the ExoMars rover ALD. However, it also  
38 397 stresses the necessity of performing the RLS automated operation. This approach (MICR-  
39 398 RLS collaborative + RLS automated acquisition) is currently foreseen in the rover software  
40 399 capabilities and is the best way to ensure a proper characterization of the sample and the  
41 400 highest scientific return from the operation on Mars.

## 42 401 **Conclusions**

43 402 The ExoMars mission rover presents a unique and unprecedented opportunity to perform  
44 403 combined analysis between complementary techniques on a planetary *in-situ* mission, at  
45 404 the same spot of the same sample. This provides also the opportunity to perform these tasks  
46 405 onboard, without the need of ground intervention. However, in order to guarantee a correct  
47 406 alignment between the different instruments of the rover laboratory, it is necessary to  
48 407 analyze a common pattern to be able to identify the relative positions of the instruments  
49 408 after landing.

50  
51  
52 409 The RLS instrument will have two different calibration targets onboard the rover. Both  
53 410 feature a small PET part as calibrant material. Due to engineering constraints, one CT will  
54 411 be used for calibration operations and pre-launch and cruise verifications, while the other  
55 412 will be used for optical health checks during nominal operation. The RLS CT team performed  
56 413 a complete suite of tests for the qualification of PET for the conditions the exploration of

1  
2  
3 414 Mars with the ExoMars rover. The PET spectrum also presents several peaks distributed  
4 415 along the spectral range as well as a characteristic background with which it will be possible  
5 416 to verify the health status and check the spectral calibration of the instrument, even at the  
6 417 different operation temperatures expected during the mission.

8 418 In order to facilitate the spatial cross-registration of the instruments, especially RLS and  
9 419 MicrOmega, one of the two CTs was modified to include patterns that can be detected by  
10 420 both instruments. These patterns were created by performing mechanical (milling) and  
11 421 molecular modifications (with laser) and will be used to correlate the positions of the  
12 422 instruments. This is key to facilitate the combined science concept onboard ExoMars.

13 423 The joint analysis performed by RLS and MicrOmega show how the combined science  
14 424 between the instruments of the rover is of paramount importance in order to increase the  
15 425 scientific return of the mission. However, these joint tests have also shown that the RLS  
16 426 instrument obtains very fruitful results when working in autonomous mode (without  
17 427 indication from other instruments), further complementing the RLS+MicrOmega combined  
18 428 operation. Therefore, the operational approach of the ExoMars has been designed to allow  
19 429 the combination of the MicrOmega-RLS collaborative operation plus an RLS automated  
20 430 acquisition.

21 431 Future work should be directed in two different lines. On one hand, performing further tests  
22 432 with the other instruments of the rover (as for example a MicrOmega, RLS and MOMA joint  
23 433 test). On the other, it is well known that the combination of Raman and infrared  
24 434 spectroscopies is very fit given the complementarity in their detection capabilities, so  
25 435 working in joint analytical techniques such as data fusion for improved analytical  
26 436 performances seems to be necessary in order to push the collaboration from a data-  
27 437 acquisition to a data-exploitation perspective.

### 33 438 **Acknowledgements**

34 439 The authors acknowledge and are very thankful to all the people that has participated in the  
35 440 development of the RLS CT, taking the work one step further than it was strictly necessary.

36 441 This work is funded by the projects from the Spanish Ministerio de Economía y  
37 442 Competitividad (MINECO) under references ESP2014-56138-C3-2-R and ESP2107-87690-  
38 443 C3-1-R.  
39  
40  
41  
42  
43  
44  
45  
46  
47  
48  
49  
50  
51  
52  
53  
54  
55  
56  
57  
58  
59  
60

444 **References**

- 445 [1] J. L. Vago, et al., *Astrobiology*. **2017**; *17*, 471.
- 446 [2] F. Rull, S. Maurice, I. Hutchinson, A. Moral, C. Perez, C. Diaz, M. Colombo, T.  
447 Belenguer, G. Lopez-Reyes, A. Sansano, O. Forni, Y. Parot, N. Striebig, S. Woodward,  
448 C. Howe, N. Tarcea, P. Rodriguez, L. Seoane, A. Santiago, J. A. Rodriguez-Prieto, J.  
449 Medina, P. Gallego, R. Canchal, P. Santamaría, G. Ramos, J. L. Vago, *Astrobiology*.  
450 **2017**; *17*, 627.
- 451 [3] J. P. Bibring, V. Hamm, C. Pilorget, J. L. Vago, MicrOmega Team, *Astrobiology*.  
452 **2017**; *17*, 621.
- 453 [4] J. P. Bibring, V. Hamm, Y. Langevin, C. Pilorget, A. Arondel, M. Bouzit, M.  
454 Chaigneau, B. Crane, A. Darié, C. Evesque, J. Hansotte, V. Gardien, L. Gonnod, J. C.  
455 Leclech, L. Meslier, T. Redon, C. Tamiatto, S. Tosti, N. Thoores, *Space Science Reviews*.  
456 **2017**; *208*, 401.
- 457 [5] C. Pilorget, J. P. Bibring, *Planetary and Space Science*. **2013**; *76*, 42.
- 458 [6] G. Fred, et al., *Astrobiology*. **2017**; *17*, 655.
- 459 [7] R. D. P. Daubeny, C. W. Bunn, C. J. Brown, W. L. Bragg, *Proceedings of the Royal*  
460 *Society of London. Series A. Mathematical and Physical Sciences*. **1954**; *226*, 531.
- 461 [8] M. R. Patel, J. C. Zarnecki, D. C. Catling, *Planetary and Space Science*. **2002**; *50*, 915.
- 462 [9] M. R. Patel, A. Bérces, C. Kolb, H. Lammer, P. Rettberg, J. C. Zarnecki, F. Selsis,  
463 *International Journal of Astrobiology*. **2003**; *2*, 21.
- 464 [10] J. E. Moores, P. H. Smith, R. Tanner, A. C. Schuerger, K. J. Venkateswaran, *Icarus*.  
465 **2007**; *192*, 417.
- 466 [11] E. Mateo-Marti, *Challenges*. **2014**; *5*, 213.
- 467 [12] E. Mateo-Martí, O. Prieto-Ballesteros, J. M. Sobrado, J. Gómez-Elvira, J. A. Martín-  
468 Gago, *Measurement Science and Technology*. **2006**; *17*, 2274.
- 469 [13] A. C. Schuerger, J. E. Moores, C. A. Clausen, N. G. Barlow, D. T. Britt, *Journal of*  
470 *Geophysical Research: Planets*. **2012**; *117*, n/a.
- 471 [14] G. Lopez-Reyes, F. Rull, G. Venegas, F. Westall, F. Foucher, N. Bost, A. Sanz, A.  
472 Catalá-Espí, A. Vegas, I. Hermosilla, A. Sansano, J. Medina, *European Journal of*  
473 *Mineralogy*. **2013**; *25*, 721.
- 474 [15] G. Lopez-Reyes, A. Perez Oliveros, A. Sanz, F. Rull In *12th International*  
475 *GeoRaman Conference*. Novosibirsk (Russia), 2016; Vol. Georaman 2016 book of  
476 abstracts, p 111.
- 477 [16] G. Lopez-Reyes, F. Rull Pérez, *Journal of Raman Spectroscopy*. **2017**; *48*, 1654.
- 478 [17] C. Pilorget, J. P. Bibring, *Planetary and Space Science*. **2014**; *99*, 7.



1  
2  
3 479 **Table 1. SNR values of the Raman spectra obtained from the RLS CT test units**  
4 480 **before and after the qualification campaign, which included -among other**  
5 481 **processes- a 150h bakeout at 125°C and a 120h sterilization process at 115°C.**  
6  
7

Point	CT3		CT4		CT5	
	Before	After	Before	After	Before	After
1	131	151	100	142	152	139
2	113	129	112	135	146	137
3	103	128	98	124	149	139
4	104	127	119	134	144	140
5	118	134	95	138	127	140
<b>Average</b>	<b>114</b>	<b>134</b>	<b>105</b>	<b>135</b>	<b>144</b>	<b>139</b>

18 482

20 483

For Peer Review

1  
2  
3 484 **Table 2. SNR values of the Raman spectra obtained from PET after the UV**  
4 485 **exposure tests. The PET1 exposed face is the upper face of the irradiated PET**  
5 486 **sample, where the UV radiation hit directly. PET1 non-exposed (shadow) refers**  
6 487 **to a region of the upper face that was shadowed from the UV radiation. The**  
7 488 **PET1 non-exposed face (lower face) corresponds to the lower face of the PET1.**  
8 489 **The PET2 non-exposed sample is the control sample, which was not introduced**  
9 490 **in the chamber.**

Point	PET1 UV exposed face	PET1 non-exposed (shadow)	PET1 non-exposed face (lower face)	PET2 non-exposed sample (control)
1	377	492	534	778
2	210	795	449	885
3	224	-	688	745
4	317	-	792	613
Average	<b>282</b>	<b>644</b>	<b>616</b>	<b>755</b>

21 491

22 492

493 **Table 3. Targets position and composition from RLS and MicrOmega analyses**  
 494 **for sample 1.**

Target name	Position in MicrOmega's frame (x,y)	Composition from MicrOmega data	Position of RLS spot in reference frame ( $\mu\text{m}$ )	Composition from RLS data
<b>Target A</b>	Pixel (89,191)	Carbonate mixed with Fe-rich smectite and gypsum	(9925,24065)	Dolomite, cerussite and gypsum
<b>Target B</b>	Pixel (202,165)	Carbonate mixed with Fe-rich and Al-rich smectites and gypsum	(10135,23690)	Dolomite
<b>Target C</b>	Pixel (221,176)	Carbonate mixed with Al-rich smectite and gypsum	(12275,23295)	Dolomite, cerussite and gypsum

495

496 **Table 4. Targets position and composition from RLS and MicrOmega analyses**  
 497 **for sample 2.**

Target name	Position in MicrOmega's frame (x,y) and corresponding position in reference frame	Composition from MicrOmega data	Position of RLS spot in reference frame ( $\mu\text{m}$ )	Composition from RLS data
<b>Target A</b>	Pixel (75,150)	Anhydrous carbonate mixed with olivine	(17085,18995)	Dolomite, and two types of olivine (forsterite and Fe-Rich olivine)
<b>Target B</b>	Pixel (140,55)	Anhydrous carbonate mixed with olivine	(15295,17930)	Dolomite and olivine (forsterite)
<b>Target C</b>	Pixel (28,88)	Carbonate with OH or H <sub>2</sub> O mixed with olivine	(17385,17620)	Dolomite and forsterite
<b>Target D</b>	Pixel (41,205)	Carbonate with OH or H <sub>2</sub> O	(18060,19640)	Dolomite and olivine (forsterite)

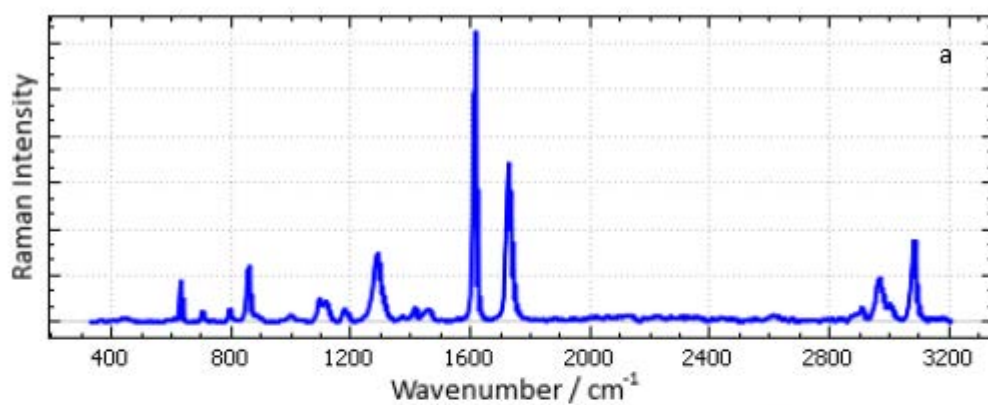
498

499

500

501 **Figure 1. PET spectrum (a). RLS calibration targets (b). RLS CT design and**  
502 **configuration, showing how the calibrant (PET, white part)**  
503 **is mechanically fixed to the CT body (c).**

504

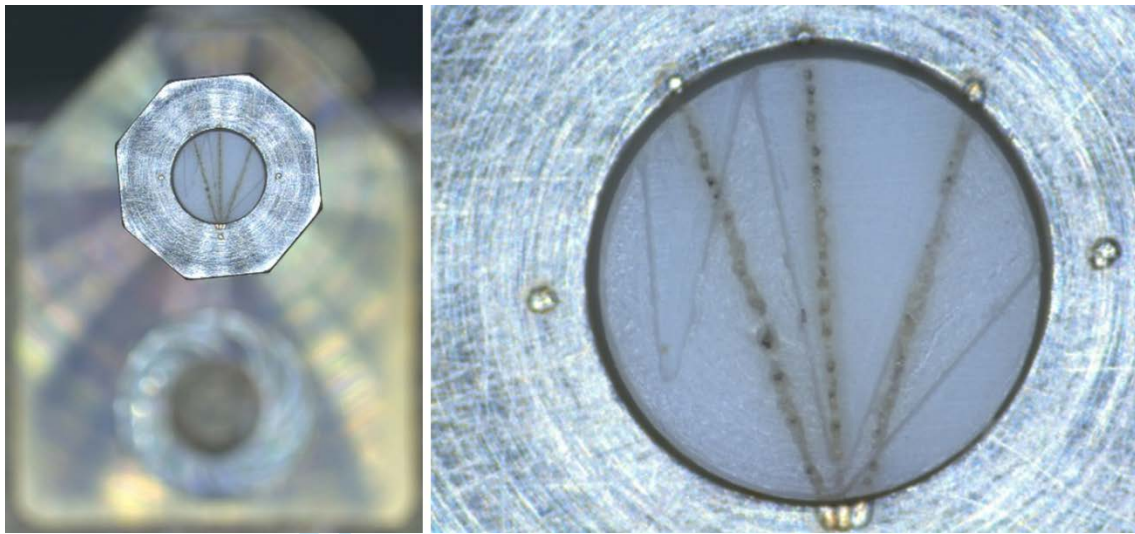


505

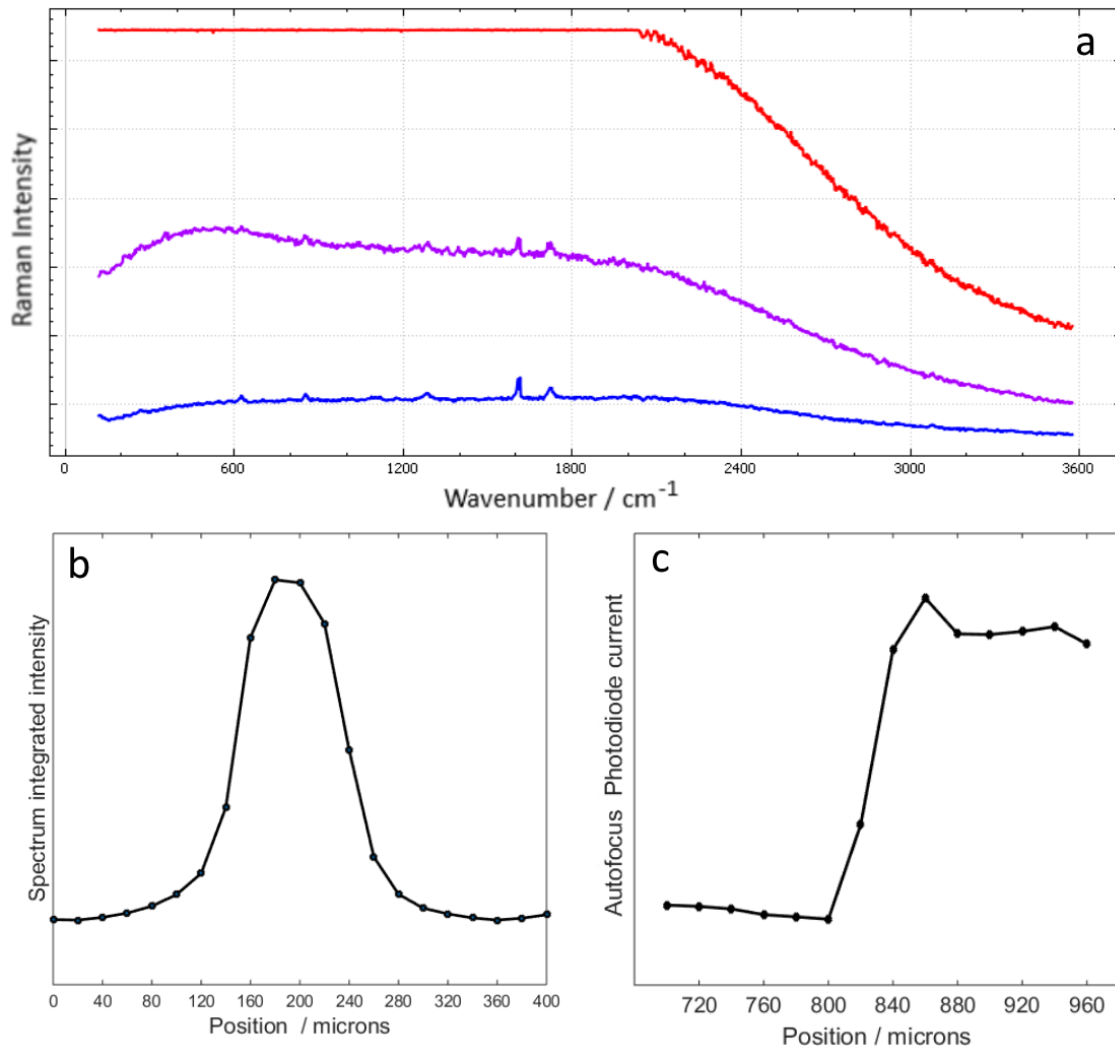
506



1  
2  
3 507 **Figure 2. RLS CT with the mechanical and laser-induced patterns.**  
4



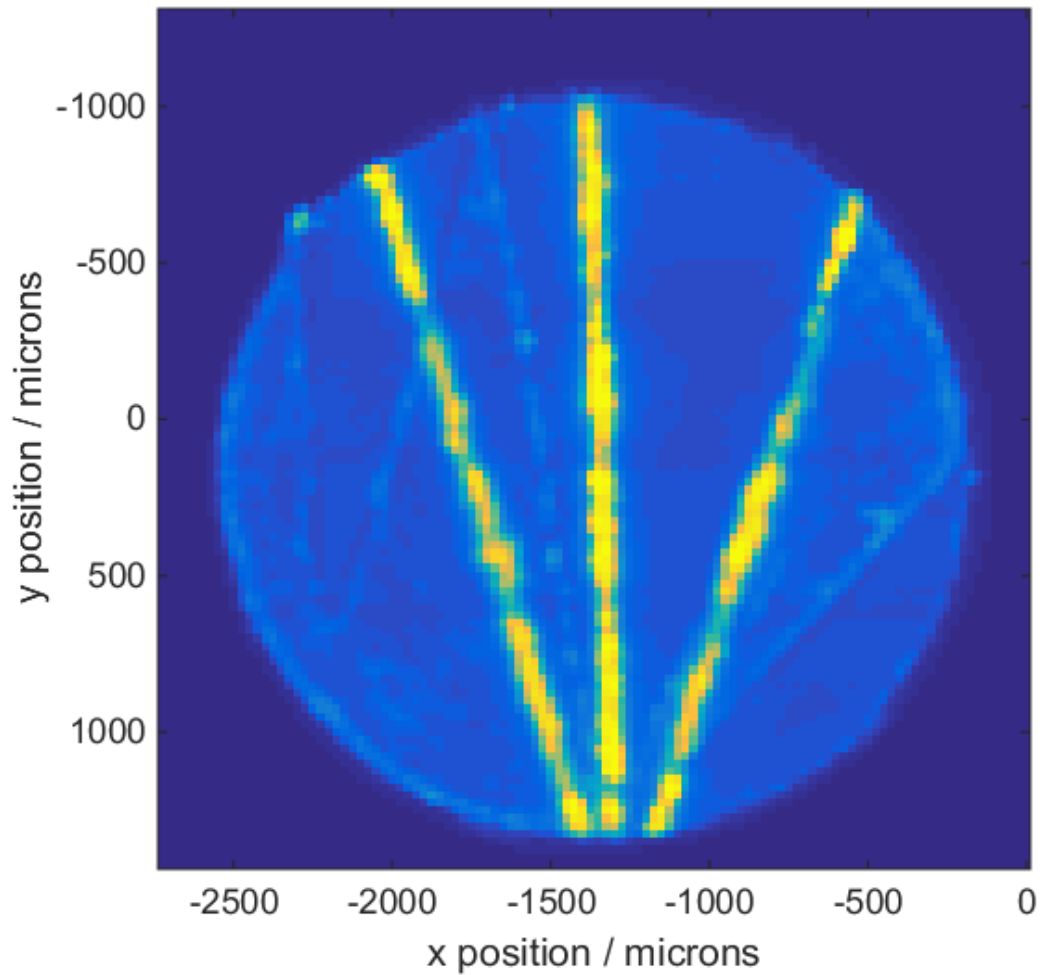
1  
2  
3 510 **Figure 3. Raman spectra examples on the marked surface(a): PET (blue), laser**  
4 **mark (red), threshold between the PET and the mark (cyan). Detection of a**  
5 **laser line by Raman spectroscopy (b). Detection of the mechanical mark with**  
6 **the RLS autofocus photodiode (c).**  
7 513



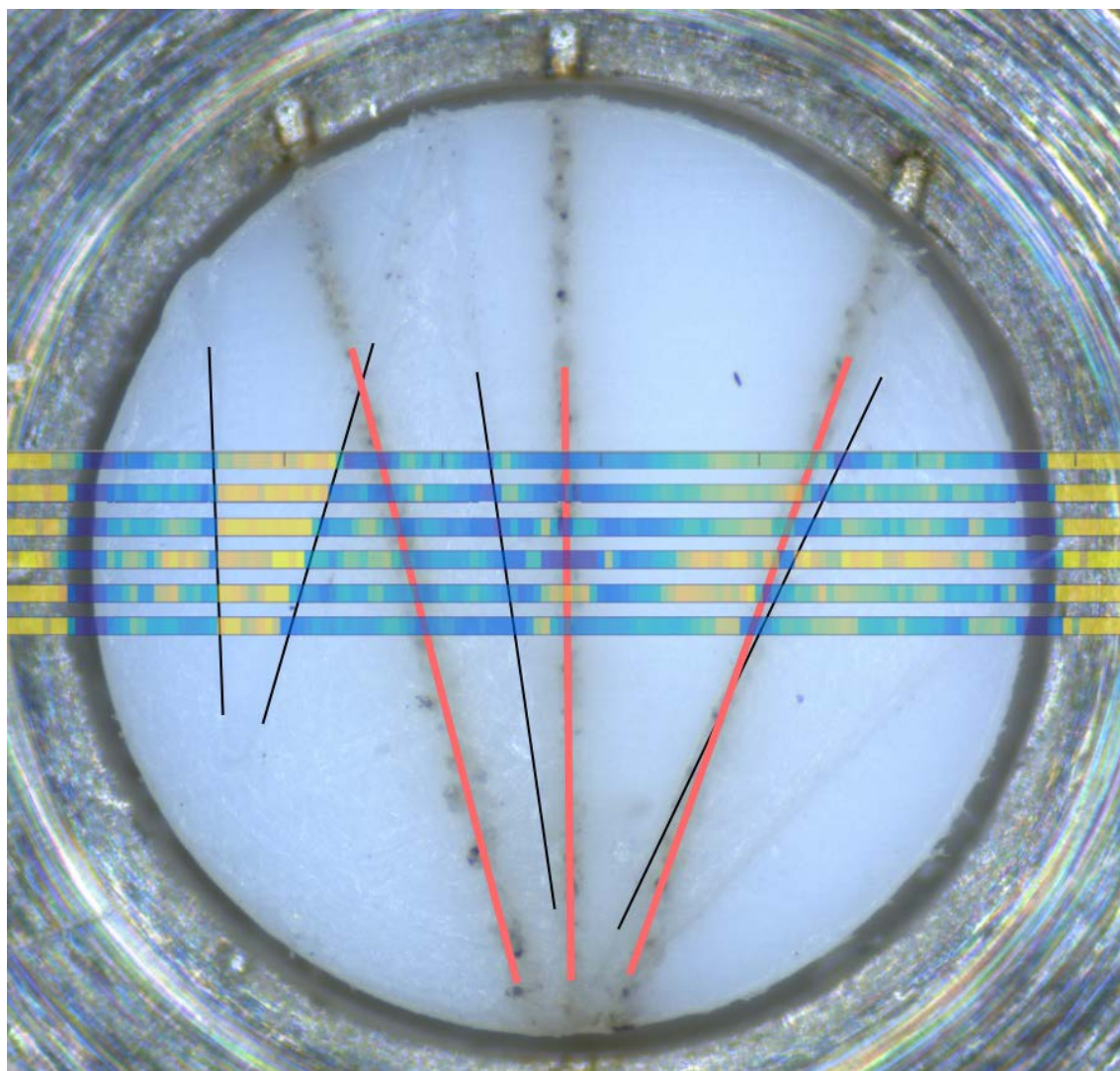
514

515

1  
2  
3 516 **Figure 4. Map of the RLS CT performed with the RLS ExoMars Simulator. Each**  
4 **pixel represents the spectrum integrated intensity. Spatial resolution is 25**  
5 **microns.**  
6  
7  
8  
9



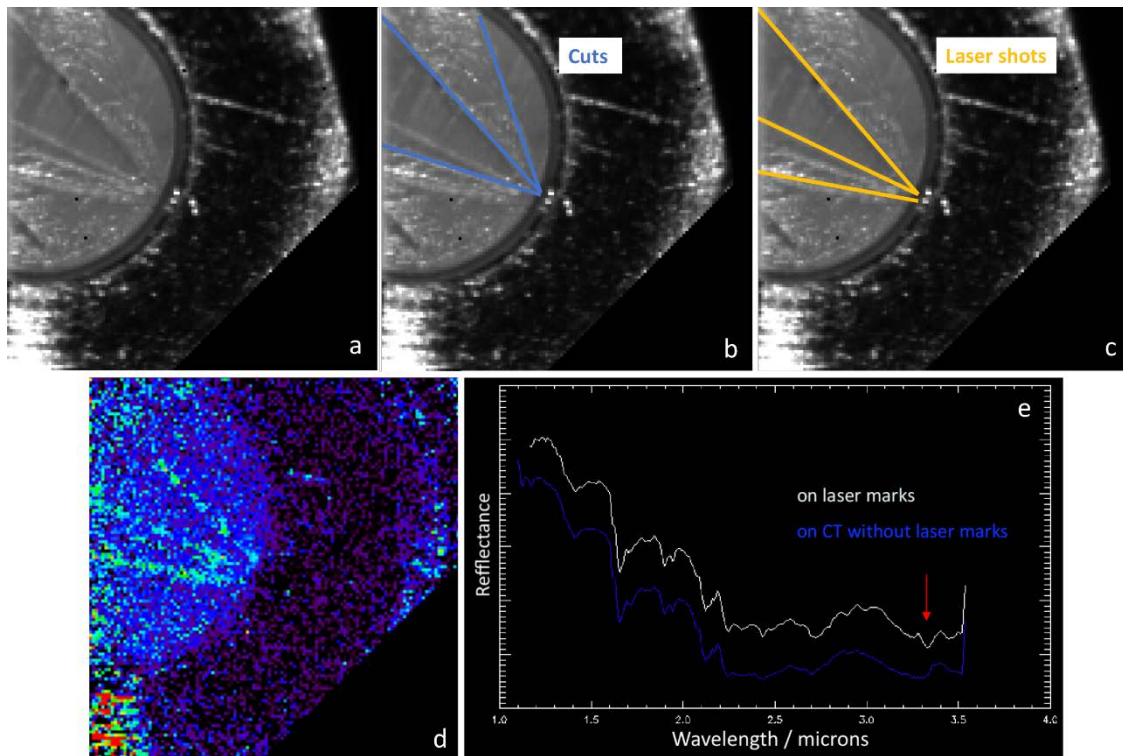
1  
2  
3 521 **Figure 5. Partial map of the CT based on the RLS autofocus photodiode**  
4 522 **intensity values. Black lines represent the borders of the mechanical marks,**  
5 523 **while the red lines represent the laser marks. Superimposed are the values**  
6 524 **from the photodiode.**  
7



41 525

42 526  
43  
44  
45  
46  
47  
48  
49  
50  
51  
52  
53  
54  
55  
56  
57  
58  
59  
60

1  
2  
3 527 **Figure 6. Map of the CT performed with the MicrOmega instrument. The**  
4 **monochromatic image at 1.3 micrometers (a) allows the identification of the**  
5 **mechanical (b) and laser marks (c). The laser lines are also detected based on**  
6 **529 their spectroscopic response (d, e).**  
7 530

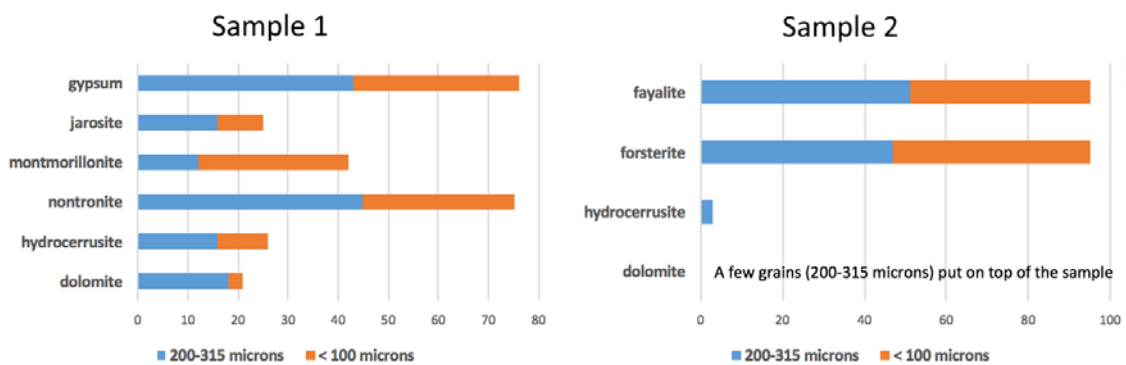


531

532



533 **Figure 7. Mass composition (in mg) of sample 1 (left) and sample 2 (right) used**  
 534 **in the RLS MicrOmega joint test.**

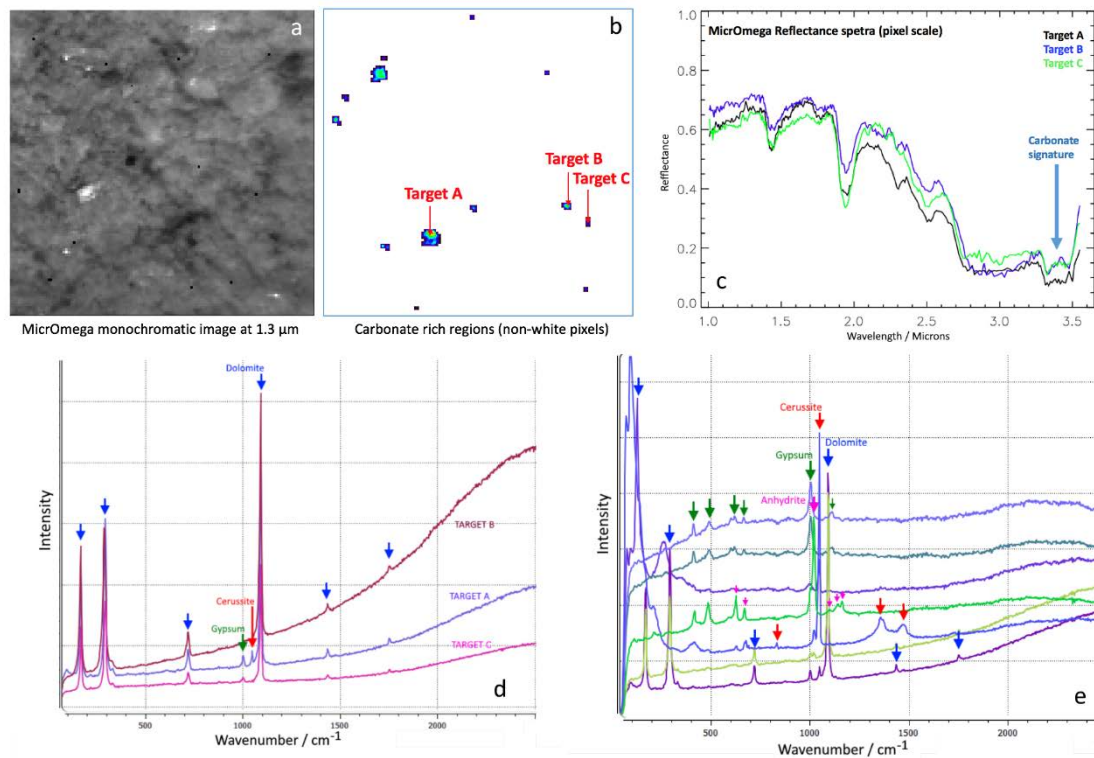


535

536

For Peer Review

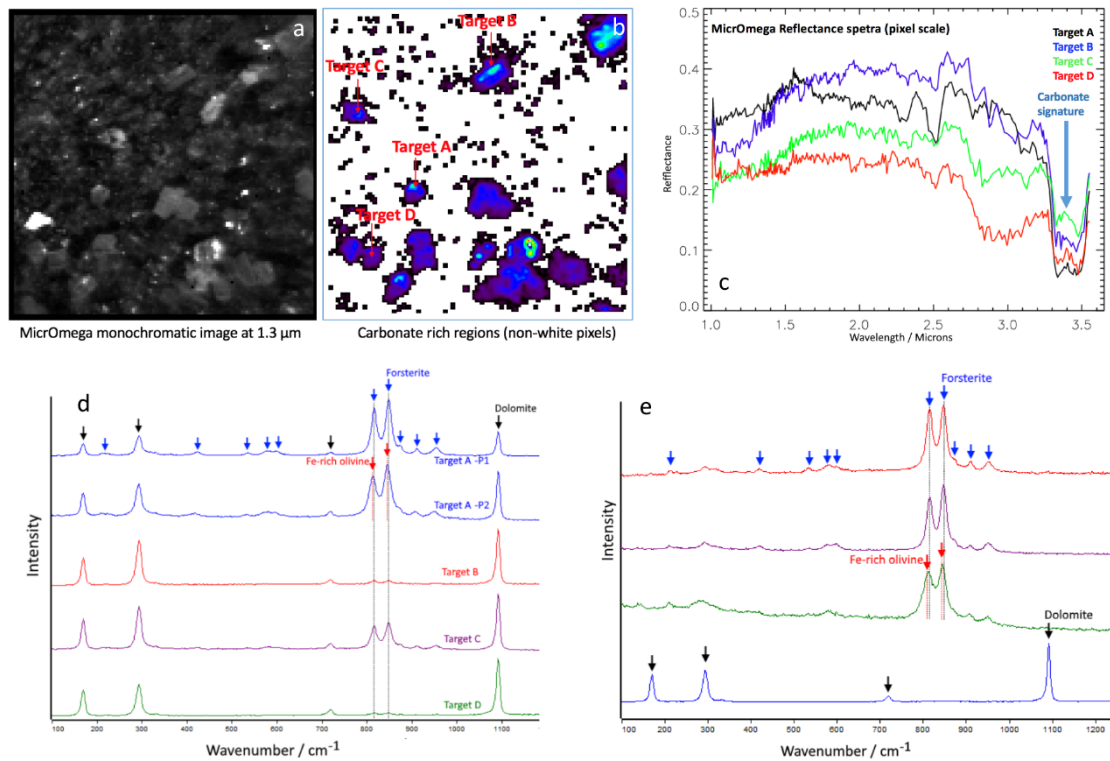
1  
2  
3 537 **Figure 8. Sample 1 analysis results. MicrOmega monochromatic image at 1.3**  
4 **micrometers (a) is used to detect features of interest -in this case, carbonates-**  
5 **(b). Reflectance spectra from MicrOmega data (c). Selection of spectra of the**  
6 **RLS analysis on the targets defined by MicrOmega (d), and from the automatic**  
7 **analysis by RLS (e).**  
8  
9



542

543

544 **Figure 9. Sample 2 analysis results. *MicrOmega* monochromatic image at 1.3**  
 545 **micrometers (a) is used to detect features of interest (b). Reflectance spectra**  
 546 **from *MicrOmega* data (c). Selection of spectra of the RLS analysis on the**  
 547 **targets defined by *MicrOmega* (d), and from the automatic analysis by RLS (e).**



548

549